Engineering with Computers

Incremental Volumetric and Dual Kriging remapping methods

--Manuscript Draft--

Manuscript Number:	EWCO-D-16-00042
Full Title:	Incremental Volumetric and Dual Kriging remapping methods
Article Type:	Original Article
Corresponding Author:	Carlos Miguel Afonso Diogo, M.D. PORTUGAL
Corresponding Author Secondary Information:	
Corresponding Author's Institution:	
Corresponding Author's Secondary Institution:	
First Author:	Carlos Miguel Afonso Diogo, M.D.
First Author Secondary Information:	
Order of Authors:	Carlos Miguel Afonso Diogo, M.D.
	Diogo Mariano Neto, Ph.D
	Marta Cardoso Oliveira, Ph.D
	José Luís Alves, Ph.D
	Luís Filipe Menezes, Ph.D
Order of Authors Secondary Information:	
Funding Information:	Fundação para a Ciência e a Tecnologia (SFRH/BPD/101334/2014) — Diogo Mariano Neto
	Fundação para a Ciência e a Tecnologia (PTDC/EMS-TEC/6400/2014) — Not applicable
	Fundação para a Ciência e a Tecnologia (PTDC/EMS-TEC/0702/2014) — Not applicable
Abstract:	The transfer of variables between distinct spatial domains is a problem shared by many research fields. Among other applications, it may be required for visualization purposes or for intermediate analysis of a process. In any case, two important factors must be considered: accuracy and computational performance. The accuracy becomes even more important when the results have an impact on the subsequent stages of the process' analysis, as it could lead to incorrect results. The computational performance is a permanent requirement due to the ever-increasing complexity of the analysed processes. The aim of this work is to present a new remapping method, based on Dual Kriging interpolation, developed to enable accurate and efficient variable transfer operations between two different domains, discretized with hexahedral finite elements. Two strategies are proposed, which take into account different selections of interpolation points and are based on specific Finite Element Method features. They are compared with the Incremental Volumetric Remapping method in two remapping examples, one of which includes a trimming operation, highlighting their advantages and limitations. The results show that the Dual Kriging remapping method can contribute to increase the accuracy and the computational performance of these operations.
Suggested Reviewers:	Ricardo J.A. de Sousa, Ph.D Universidade de Aveiro rsousa@ua.pt Researcher with several publications in the field of incremental forming process, including numerical simulation involving remeshing procedures.
	Paulo A.F. Martins, Ph.D

	Instituto Superior Técnico, Universidade de Lisboa pmartins@ist.utl.pt Researcher with deep knowledge on the numerical simulation of metal forming processes involving remeshing prcedures.
	François Trochu, Ph.D Ecole Polytechnique de Montreal francois.trochu@polymtl.ca Researcher with several publications in the field of applications of kriging in engineering.

Incremental Volumetric and Dual Kriging remapping methods

C.M.A. Diogo[a,1], D.M. Neto[a], M.C. Oliveira[a], J.L. Alves[b], L.F. Menezes[a]

[a]CEMUC, Department of Mechanical Engineering, University of Coimbra, Polo II, Rua Luís Reis Santos, Pinhal de Marrocos, 3030-788 Coimbra, Portugal

[b]MEMS, Microelectromechanical Systems Research Unit, University of Minho, Campus de Azurém, 4800-058 Guimarães, Portugal

Abstract

The transfer of variables between distinct spatial domains is a problem shared by many research fields. Among other applications, it may be required for visualization purposes or for intermediate analysis of a process. In any case, two important factors must be considered: accuracy and computational performance. The accuracy becomes even more important when the results have an impact on the subsequent stages of the process' analysis, as it could lead to incorrect results. The computational performance is a permanent requirement due to the ever-increasing complexity of the analysed processes. The aim of this work is to present a new remapping method, based on Dual Kriging interpolation, developed to enable accurate and efficient variable transfer operations between two different domains, discretized with hexahedral finite elements. Two strategies are proposed, which take into account different selections of interpolation points and are based on specific Finite Element Method features. They are compared with the Incremental Volumetric Remapping method in two remapping examples, one of which includes a trimming operation, highlighting their advantages and limitations. The results show that the Dual Kriging remapping method can contribute to increase the accuracy and the computational performance of these operations.

Keywords: Finite Element Method, Remapping, Dual Kriging, Trimming, Hexahedral finite element

1. Introduction

Engineers have always been drawn to solve complex problems. The Finite Element Method (FEM) emerged in the sixties, enabling the solution of problems that could not be solved analytically [1, 2]. Nowadays, the FEM is used in diverse engineering fields [3–6], specifically in most engineering companies and research centres, which resort to commercial or in-house FEM solvers. Whatever the application field, FEM requires the partition of the spatial domain into smaller parts, known as finite elements, which define the mesh that approximates the original domain. The type of finite elements used can depend on the application field or problem, e.g.

[1]Corresponding author at: CEMUC, Department of Mechanical Engineering, University of Coimbra, Polo II, Pinhal de Marrocos, 3030-788 Coimbra, Portugal. Tel.: +351239790700, Fax: +351239790701.
E-mail addresses: papers.diogocma@gmail.com (C.M.A. Diogo), diogo.neto@dem.uc.pt (D.M. Neto), marta.oliveira@dem.uc.pt (M.C. Oliveira), jlalves@dem.uminho.pt (J.L. Alves), luis.menezes@dem.uc.pt (L.F. Menezes)

[7], which can vary between 1-D, 2-D and 3-D, using interpolation functions of different degrees. The linear isoparametric hexahedral and tetrahedral finite elements are commonly used in 3-D simulations, adopting different mesh topologies, rendering coarser or finer spatial discretizations.

The solution of nonlinear problems also requires the division of the temporal domain to take into account time dependant variables [3–6], which can be related to geometrical, material or boundary conditions nonlinearities. Typically, resorting to more divisions – spatial and temporal – increases the accuracy of the numerical results, but increases the computational cost [8, 9]. Therefore, it is always necessary to find the best compromise between results accuracy and computational effort. In terms of spatial discretization, the definition of zones with different mesh sizes can be performed either in the pre-processing stage or during the numerical simulation. The definition of different zones in the pre-processing is usually carried out manually, which contributes to an increase of the time required for this stage. On the other hand, during the numerical simulation, the definition of different zones requires the application of adaptive mesh refinement/remeshing algorithms [6, 10], in several temporal increments. The finite elements are divided or combined depending on predefined conditions (e.g. high value of strain [6] and/or high element distortion [11, 12]) in order to provide good results while ensuring computational efficiency [8, 10]. In fact, adaptive mesh refinement algorithms are commonly used to overcome problems of excessive distortion/deformation of the finite elements, which occur in different forming processes [6, 10, 13–15], such as forging, and sheet metal forming. The adaptive mesh refinement is usually performed by one of three methods: p-adaptive (change of the interpolation degree), h-adaptive (change of the element size), r-adaptive (change of the nodes location); or by a combination of them [10]. The improvement of these methods is an up to date research topic in computational mechanics, since small improvements have a considerable impact on computational performance, due to being applied several times during the simulation.

The adoption of adaptive mesh refinement algorithms involves a remapping step, i.e. the transfer of variables between different spatial discretizations [6], which can present a strong influence in the accuracy of the results and computational efficiency. Nonetheless, in some increments the zone to be remapped can be localized, as in the numerical analysis of trimming operations involved in some multi-stage forming processes. Typically, a simplified approach is used to model these operations, which consists in the geometrical trimming operations of the FE mesh [16]. Thus, after each trimming operation it is also necessary to perform a remapping procedure for the numerical variables involved in the subsequent forming steps. In this case, the impact of the selected remapping method on the computational efficiency is insignificant, but its accuracy can have a strong influence in the results of the subsequent numerical simulation. When using the FEM, it can be necessary to transfer the nodal variables (primary unknowns), such as forces and displacements; and the state variables (secondary unknowns), that are evaluated in the integration points (typically Gauss points), such as the stress and strain state. Firsts are usually continuous while seconds are discontinuous (e.g. [6]).

Jiao and Health [17], divide the remapping methods into four major groups. The first group refers to pointwise interpolation and extrapolation methods, such that the variables are transferred using a function that interpolates/extrapolates the variables from the donor mesh to the target, in one or more stages. The pointwise interpolation can be categorized into two types of interpolants: (i) use of the same function as the one for the donor mesh (sometimes referred to as consistent interpolation or inverse isoparametric mapping (e.g.: [18, 19])) and (ii)

use of basis functions of higher order than the one of the donor basis. According to Batista [20], taking into account the mathematical characteristics of these methods, this group can also include the ones based on the application of the moving least squares [13, 21] and the Superconvergent Patch Recovery methods, developed by Zienkiewicz and Zhu [22]. The second group refers to Area/Volume weighted averaging methods (also referred as Finite Volume Transfer Method in [14]), which uses a transfer function that is evaluated based on the area/volume of intersection between the donor and the target FE. These areas/volumes act as a weighting factor defining the contribution of each donor element to the target one (e.g. [23, 24]). The third group refers to Mortar element methods, which are general techniques for projecting data at interfaces between two or more non-conforming subdomains [14]. From a mathematical point of view, this method consists in the minimization of a weighted residual, where the weight functions are usually chosen from the space spanned by the basis functions of the mortar side [25]. The last group refers to specialized methods, which are designed for specific applications and do not fall directly into the above categories, but frequently are variants or combinations of them. This fourth group includes the direct allocation to the target point of the closest donor point [26], the use of different methods according to the type of variable [15], and adaptations of the interpolation/extrapolation and area/volume weighted averaging methods; by including constraints [27]; and/or considering specific features of the application domain or problem [28, 29].

2. Remapping Methods

The accurate transfer of variables between different spatial discretizations is imperative, independently of the remapping method adopted. Moreover, its computational performance is particularly important when the procedure is performed several times, whereas the error is accumulated to the following stages (e.g. [6, 14]). In fact, the remapping operation can introduce errors due to the approximations used to estimate the values for the target mesh. In order to try to control and minimize the unavoidable errors when performing remapping operations, several authors [14, 17, 19, 21, 27] point out some desirable characteristics. The method should be self-consistent such that when the target and the donor point are coincident, the transfer remapping function reduces to the identity operator (zero error). The interpolation/extrapolation methods that resort to the donor shape functions cannot guarantee, *a priori*, this condition [21]. On the contrary, Area/Volume weighted averaging methods automatically verify this self-consistence condition. The method should also guarantee the locality, i.e. the remapped value in a target point should only be affected by the variables of the donor mesh in a region of influence. This assures the preservation of discontinuities, related with material or geometric interfaces, which must also be present in the remapped mesh. However, due to the discrete and approximated natured of the remapping operations, it is always expected some degradation (smoothing) of the variable when severe gradients are present. Nonetheless, the smoothing should be minimized in order to preserve, as accurately as possible, the gradients of the donor mesh. On the other hand, the remapping method can also lead to spurious local extreme values, which are non-physical and result in the degradation of the numerical simulation result. Accordingly, the remapping algorithm should allow for the inclusion of some constraints, such as consistency of equilibrium or motion equations [27], consistency between the displacement field and the stress state [19] or boundary conditions [19].

In order to take advantage of the characteristics of these applications, several specialized remapping methods have been proposed in order to find the best compromise between accuracy and computational performance. One example is the application of the moving least squares method, proposed by Rashid [21], based on a transfer function. It tries to force the equality between the variable field in a volumetric domain of the donor and of the target mesh, assuming that each donor integration point has constant state variables in a predefined region. Jiao and Heath [17] present a general method, named Common Refinement, which is based on the intersection of the donor and target mesh in order to define a third mesh, used as an auxiliary for the transfer procedure. The main advantage of this method is that it allows the accurate integration of the transfer function, which depends on the shape functions of the target and donor meshes. However, it requires a robust and expeditious algorithm for mesh intersection, which is considerably challenging to attain when working with solid hexahedral finite elements. In this context, also the Incremental Volumetric Remapping (IVR) method was developed and applied specifically for the transfer of variables between meshes composed of linear isoparametric hexahedrons [30, 31]. This volume-weighted averaging method assumes that each donor integration point has constant state variables in a predefined region [21]. Being a volume-weighted averaging method, some of the desirable characteristics are inherently verified (self-consistency, locality and inexistence of spurious local extrema values), which make it particularly interesting for FEM analysis.

The Dual Kriging method is adopted in the present study to develop a new remapping method, which is dedicated to finite element meshes composed by isoparametric hexahedrons. This interpolation method is known for being simple, while incurring a small computational cost in the interpolation of space-dependent variables [32–35]. Both the Incremental Volumetric and the Dual Kriging remapping methods are described in the following sections. These remapping methods are implemented in the in-house code DD3TRIM, specifically developed to perform trimming and remapping operations, allowing the comparison in terms of accuracy and computational efficiency. Two examples are selected to perform the comparison between the two remapping methods: the first comprises an analytical function distribution, which is mapped between two different finite element meshes, while the second example covers a trimming operation performed on a metallic sheet.

2.1. Incremental Volumetric Remapping (IVR)

This method is based on the finite element discretization and the Gaussian quadrature rule, establishing that variables values in the region of a Gauss volume (an eight part of the standard brick element) are equal to the state variable quantity placed in the correspondent Gauss point [21]. The subdivision of a finite element into eight Gauss volumes is presented in Fig. 1. Accordingly, the variable value assigned to a given Gauss point of the target (new) mesh element is determined based on a weighted average of the values of the donor (old) mesh. The weight function should reflect the fraction of the Gauss volume of each donor element located inside the target Gauss volume (Gauss point in evaluation). However, this strategy carries the difficult problem of calculating intersecting elements volumes belonging to distinct meshes (see Fig. 2) [21, 36]. This issue is overcome by using an incremental volumetric scheme [13] to determine the intersecting volume between two finite elements.

The procedure starts with the division of both finite element meshes in Gauss volumes as shown in Fig. 1 (a) and (b). Subsequently, the Gauss volumes of the target mesh are divided in a

predefined number of parts (Fig. 1 (c)), defined by the nl parameter. The centroid of each small part of the target Gauss volume is evaluated resorting to the parametric inversion of the shape functions. To define which donor Gauss volume contains this centroid (Fig. 2 (c)), the volume coordinates method is applied. This straightforward method avoids higher time consuming iterative algorithms, such as the ones based in the parametric inversion of the element shape functions [13]. The state variable assigned to each single target Gauss volume part is equal to the one of the donor Gauss volume, in which the volume part centroid is located, as shown in Fig. 2 (c). The number of donor Gauss volumes that contributes for the target Gauss volume (in evaluation) is given by the parameter ng , which, for the example presented in Fig. 2 (c), is equal to two. The value α of the state variable in a Gauss point of the target element is given by:

$$\alpha = \sum_{i=1}^{ng} \frac{\sum_{j=1}^{nl^3} V_{j,i}}{V_{tot,i}} \alpha_i \,, \tag{1}$$

where $V_{j,i}$ is the j Gauss volume part of the target mesh contained in the donor Gauss volume i ; $V_{tot,i}$ and α_i are the total volume and the state variable quantity of the i donor Gauss volume, respectively. Note that, since each target Gauss Volume is subdivided in nl equal subdivisions in each direction, it yields a total of nl^3 divisions per element (Fig. 1 (c)). In brief, the volumetric weighting of the variables in the new mesh (Fig. 2 (c)) is given by the intersection between the donor Gauss volumes and the centroid of each subvolume. Previous results indicate that the nl parameter allows the control of the remapping accuracy required for the remapping operation. The increase of the nl parameter increases the computational time exponentially, while the error reduction stabilizes for values greater than 5 [20, 31]. Thus, in this work this value is assumed.

The IVR method has been previously implemented in the in-house code DD3TRIM, which has been specifically developed for performing geometrical trimming operations of 3D meshes, composed by linear isoparametric hexahedrons [20, 30, 31]. In sheet metal forming operations, these type of elements are typically used with a selective reduced integration scheme [37]. Thus, for each element, the state variables are evaluated in eight different integration points, also called Gauss Points (GPs) since their spatial positions in the finite element's natural coordinates are defined by the Gauss Quadrature Rule [3, 5]. In previous works, the performance of the IVR algorithm was compared with the classic interpolation/extrapolation method, using a transfer function based on the shape function of the linear isoparametric elements. Additionally, it was compared with the moving least square interpolation method, using an exponential based curve as weight function [20]. The results show that the error associated to IVR is lower when compared to these other two methods, particularly when increasing the number of consecutive remapping operations. In addition, the IVR method is robust in critical situations, such as poor geometrical definition of the mesh domain boundaries, where some nodes of the target mesh fall outside the donor mesh. However, concerning the computational cost, it was observed that the classical extrapolation/interpolation method was clearly the fastest, while the IVR method and the one based on moving least squares interpolation presented similar results [20, 30, 31].

2.2. Dual Kriging Method (DK)

Kriging is a geostatistical method developed by Krige [38] and Matheron [39]. This method and consequently the ones based on it, present two main characteristics: it is the best linear unbiased estimator of a variable and also an exact interpolator. The exact interpolator property ensures that, when the original coordinates are provided, the interpolation method will return the original values (self-consistency). The Dual Kriging version is applied in the present study as it provides an explicit parametric interpolation formula to compute the interpolation value α for any point with Cartesian coordinates $\boldsymbol{x}_t = [x \quad y \quad z]^T$ [32, 40, 41]. In the context of this work, this point denotes the target Gauss point (GP). The interpolation function can be decomposed in two terms:

$$\alpha(\boldsymbol{x}_t) = d(\boldsymbol{x}_t) + f(\boldsymbol{x}_t) \tag{2}$$

The first term, the drift, $d(\boldsymbol{x}_t)$ represents the average or global trend of $\alpha(\boldsymbol{x}_t)$ and is usually a linear polynomial function, obtained from a scalar product such as:

$$d(\boldsymbol{x}_t) = \mathbf{d}^T \cdot [1 \quad \boldsymbol{x}_t^T] = d_1 + d_2 x + d_3 y + d_4 z\,, \tag{3}$$

where $\mathbf{d}$ is the vector composed by the coefficients that define the average plane obtained from the known values at the seed points, i.e., donor GPs. Thus, the linear drift is correlated to this plane. In 2-D applications, the last term of $\boldsymbol{x}_t$, z, and of $\mathbf{d}$, d_4, are removed. The second part of the equation (2), $f(\boldsymbol{x}_t)$, represents the fluctuation or deviation from $d(\boldsymbol{x}_t)$, associated with each seed point:

$$f(\boldsymbol{x}_t) = \sum_{i=1}^{n} \lambda_i K(h_{ti}) = \sum_{i=1}^{n} \lambda_i K(|\,\mathbf{x}_t - \mathbf{x}_i\,|)\,, \tag{4}$$

where n is the total number of seed points, i.e. donor GPs; K is the generalized covariance function, which can assume different forms, but it is always a function of the Euclidean norm (h_{ti}) between the target GP (t) and each donor GP (i); and λ is a weighting factor associated with each donor GP. Thus, the general form is obtained by substituting equations (3) and (4) into equation (2):

$$\alpha(\boldsymbol{x}_t) = d_1 + d_2 x + d_3 y + d_4 z + \sum_{i=1}^{n} \lambda_i K(|\,\mathbf{x}_t - \mathbf{x}_i\,|)\,. \tag{5}$$

To obtain the value of this function, it is necessary to solve a system of linear equations of order $n+s+1$, where s defines the space dimension. This system is given by:

$$\mathbf{K}\mathbf{u} = \mathbf{f} \Leftrightarrow \mathbf{u} = \mathbf{K}^{-1}\mathbf{f}\,, \tag{6}$$

where $\mathbf{K}$ is called the Kriging matrix, $\mathbf{u}$ is the vector of unknowns, and $\mathbf{f}$ contains the values of the variable in the seed points (for further details see e.g., [32, 40, 41]). The vector of unknowns is composed by the n weighting factors λ_i and the s scalar quantities that define vector $\mathbf{d}$. The symmetric square dense matrix **K,** with null diagonal, can be divided into four submatrices, each with a different dimension, such as:

$$\begin{bmatrix} \mathbf{K}_{11} & \mathbf{K}_{12} \\ \mathbf{K}_{21} & \mathbf{K}_{22} \end{bmatrix} \times \mathbf{u} = \mathbf{f} \Leftrightarrow \left[\begin{array}{ccc|ccc} & K\left(\left|\mathbf{x}_i - \mathbf{x}_j\right|\right) & & 1 & \mathbf{x}_1^{\mathrm{T}} \\ & & & \vdots & \vdots \\ & & & 1 & \mathbf{x}_n^{\mathrm{T}} \\ \hline 1 & \cdots & 1 & 0 & \cdots & 0 \\ \mathbf{x}_1 & \cdots & \mathbf{x}_n & \vdots & \ddots & \vdots \\ & & & 0 & \cdots & 0 \end{array}\right] \times \begin{bmatrix} \lambda_1 \\ \vdots \\ \lambda_n \\ d_1 \\ \vdots \\ d_s \end{bmatrix} = \begin{bmatrix} \mathrm{f}_1 \\ \vdots \\ \mathrm{f}_n \\ 0 \\ \vdots \\ 0 \end{bmatrix}, \quad (7)$$

where $\mathbf{K}_{11}$ is the bigger submatrix, with dimension $n \times n$, containing the covariance values between each donor point, i.e., $\mathbf{K}_{11} = K\left(h_{ij}\right)$, $i, j = 1,...,n$. As previously mentioned, these values depend on the covariance function selected. $\mathbf{K}_{21} = \mathbf{K}_{12}^{\mathrm{T}}$, is a matrix with dimension $\left(s+1\right) \times n$, with the first row equal to one and the coordinates x, y and z of each donor GP in the second, third and fourth column, respectively. The number of rows of this matrix depends on the space dimension $s+1$. $\mathbf{K}_{22}$ is a square matrix with the same dimension as the number of rows of $\mathbf{K}_{21}$, $\left(s+1\right) \times \left(s+1\right)$, and always contains only null values.

The accuracy of the results provided by the Dual Kriging method is significantly affected by the covariance function selected, as shown by McLean et al. [32]. They compared three different functions and concluded that the best was simply given by the Euclidean distance, which is also adopted in the present work:

$$K(h) = h = \left|\boldsymbol{x}_{\mathrm{t}} - \mathbf{x}_j\right|. \quad (8)$$

The (Dual) Kriging is a global interpolation method, i.e. the interpolation function can be evaluated only once for the whole domain using the information of all donor points [32, 34, 41]. Nevertheless, this procedure is not mandatory which can help save some computational time. Furthermore, whatever the number of donor points selected, as long as this set remains unchanged, once the Kriging matrix is inverted (see equation (6)), it is only necessary to update the values of the variable to be remapped from the donor GP points (vector $\mathbf{f}$) in order to attain the coefficients necessary to evaluate its value for the target (using equation (5)). Thus, unlike the strategy adopted in the IVR method, where the same weight value is applied in the remapping of all state variables, Kriging interpolation evaluates the drift and the fluctuation (see equation (2)) associated with each state variable. The computational performance of the Dual Kriging method depends on the size of the linear system of equations to be solved, which in turn depends on the number of donor GPs (n) selected to interpolate each target GP. Direct inversion can be applied for small rank matrixes, but bigger require a direct or an iterative solver, due to the non-linear scaling of the required computational time of the first option. In this work, the system of linear equations (see equation (6)) is solved through the matrix inversion, since this enables a faster evaluation of the Kriging interpolation parameters for several state variables, as long as the set of donor GPs remains unchanged, as previously mentioned.

The implementation of Kriging as a remapping method, applied to each target GP, can be divided into three stages: (i) selection of a set of neighbour donor GPs; (ii) evaluation of the Kriging coefficients and weighting factors; and (iii) evaluation of each state variable value in the target GP. In the first stage, similarly to many numerical methods that allow for a flexible amount of inputs, the problem of overfitting or underfitting is present. Generally, overfitting can occur

when a mathematical function is forced to intercept too many points, while underfitting occurs when there are not enough points to provide a good representation of the domain. It is also important to consider the discontinuous nature of the variables, since continuity is ensured inside the element but not outside. These two factors oppose the use of a brute force method, i.e. simultaneous use of all donor mesh's GPs. Thus, the alternative is to search for a limited number of donor GPs in the neighbourhood. Besides improving accuracy, this also reduces the computational cost of the method, particularly by constraining the number of seed points.

Several selection algorithms for choosing the set of donor GPs were tested, being the most promising the ones referred as Master-Slave and Planar methods, which will be described in the following (for further details please refer to Diogo [42]). Both involve the knowledge of the mesh connectivity and the evaluation of the Cartesian coordinates of the donor and target GPs, enabling the subsequent assembly of the Kriging matrix $\mathbf{K}$, its inversion in the second stage of the remapping method, and use of the calculated values to evaluate the state variable(s) for the target GP. The foremost nomenclature used by both selection methods is defined in Table 1.

2.2.1. Master-Slave selection method

The Master-Slave method tries to avoid underfitting, overfitting and discontinuity problems, while keeping the selection method simple and efficient, by considering the connectivity of the donor finite element mesh. As previously mentioned, this procedure is based on the relative position of the target GP in the donor mesh. Thus, the nearest node of the donor mesh to the target GP is determined to define the Master Node. The selection of the Master node allows the definition of the donor finite element, based on the donor mesh connectivity and the parametric inversion of the shape functions. The donor finite element that contains the target GP is defined as the Master Element and all other elements that share the Master Node are defined as Slave Elements. Fig. 3 (a) shows an example of the selection of GPs from the Slave Elements, for a target GP located inside a Master Element, which corresponds to the left inferior posterior quadrant (omitted to simplify the visualization). The set of donor GPs (see Fig. 3 (a)) is composed by: (i) eight GPs of the Master Element (omitted); (ii) four GPs of each Slave Element with only one shared face (in blue); (iii) two GPs of each Slave Element with only one shared edge (in green); and (iv) one GP of each Slave Element with only one shared vertex (in red). For this example, the set of donor GPs is composed by eight GPs from the Master Element and nineteen from the Slave Elements, i.e. $n = 27$. Therefore, in this work the Kriging matrix is directly inverted due to its small overall size.

2.2.2. Planar selection method

This selection method is an alternative to the Master-Slave, where only the GPs located in the same layer are considered. Thus, although similar to Master-Slave, it does not consider the influence of GPs located in layers different from the target GP. For a target GP located in the same position, the set of selected donor GPs (see Fig. 3 (b)) is composed by: (i) four GPs of the Master Element located in the same reference face (in blue); (ii) two GPs of each Slave Element with one shared edge with the reference face (in green); and (iii) one GP of each Slave Element with one shared vertex with the reference face (in red). Thus, for the same target GP used in Fig. 3 (a), the planar method leads to nine donor GPs, i.e. $n = 9$, as shown in Fig. 3 (b).

Two implementations were tested for the planar selection remapping method, the difference being the spatial domain: $\mathbb{R}^3$ and $\mathbb{R}^2$. In the first approach the 3D Cartesian coordinates of each GP were supplied directly, i.e., the dimension of the $\mathbf{K}_{21} = \mathbf{K}_{12}^{\mathrm{T}}$ matrix was $n \times (3+1)$. However, since the foundation for this method is that the reference plane is the same, the 3-D coordinates can be converted to a plane and then converted to a 2-D coordinate system, leading to a matrix of dimension equal to $n \times (2+1)$. To evaluate this reference plane, two vectors are created based on the Master GP and the two GPs belonging to adjacent edges. The cross product of these two vectors defines the normal vector, perpendicular to the reference plane, which in turn contains the initial vectors. To correct offsets from this reference plane to GPs of the adjacent elements, two correction methods were evaluated: the projection of the converted coordinates along the normal vector and the rotation about the nearest initial vector. Due to similar results, the results presented in this work adopt the projection to the 2-D plane.

Regarding the two spatial domain implementations ($\mathbb{R}^3$ and $\mathbb{R}^2$), for the tested examples, it was found that the conversion to a 2-D coordinate system provides more accurate results, since the first can introduce some spurious gradients, due to the poor conditioning of the matrix, as there will be two linearly dependent rows (and columns): the row of ones and the row that defines the constant coordinate.

3. Remapping Examples

This section presents the comparison of both forms of the Dual Kriging remapping method with the IVR method, both in terms of computational cost and accuracy. The first example analysed deals with remapping between two different finite element meshes, which are composed by hexahedral elements (eight nodes and eight GPs). The geometry studied is a cylinder with 100 mm of radius and 1 mm of thickness, which is discretized with both in-plane structured and unstructured meshes, as shown in Fig. 4. The remapping is carried out in two stages, first, from the structured to the unstructured mesh (called *stage 1*) and afterwards, back to the structured mesh (called *stage 2*). In order to quantify the error associated with the remapping method, both meshes were initially mapped to the following scalar analytical function [14, 16, 20, 21, 31]:

$$T(r,\theta) = 20r^2(r-1)^2\cos(2\theta)\,,\; r = \sqrt{\frac{x^2+y^2}{a^2}}\,, \tag{9}$$

where r and θ are the polar coordinates, x and y the Cartesian coordinates of each GP, and a is the radius of the cylinder. Based on this definition, the absolute error associated with the remapping method E is defined as:

$$E(r,\theta) = T(r,\theta) - \alpha(\mathbf{x}_t)\,, \tag{10}$$

where T is the exact value given by the analytical function (9) and α is the interpolated value provided by the remapping method. First, the analytical distribution is considered uniform through-thickness, while a gradient along the thickness is considered in the second example, i.e. the value of T is multiplied by a coefficient depending on the position of the GP along the thickness direction. Since both finite element meshes consider two layers through-thickness (four GPs along this direction), the distribution with a through-thickness gradient assumes that

the values, from the top to the bottom layer, are equal to: T , $0{,}1\times T$, $-0{,}1\times T$, and $-T$. Fig. 4 presents the global information of both meshes and the mapped distribution. Due to how the in-plane size of the elements changes between both meshes, this can also be interpreted locally as a mesh refinement and derefinement operation.

3.1. Accuracy

The accuracy of the remapping methods is evaluated through the error analysis. Fig. 5 presents the error distributions provided by each remapping method for the case without gradient along the thickness. The presented contour plots are obtained with the GID post-processor [43] using the input values given in the GPs, which are smoothed to the mesh surface. Concerning the first remapping operation (*stage 1*), both Dual Kriging remapping methods (Master-Slave and Planar) provide similar error distribution, as shown in Fig. 5 (a). The increased error values occur close to the outer boundary, which result from the extrapolation due to the difference in the in-plane mesh size between the original mesh and the target mesh. On the other hand, the IVR method is less sensitive to the change of the in-plane mesh size, presenting a uniform error distribution in the outer boundary (see Fig. 5 (a)). In this case, the maximum error values are located near the zone where the change in mesh topology occurs in the donor mesh. Regarding the second remapping operation (*stage 2*), both Dual Kriging remapping strategies provide similar results, as shown in in Fig. 5 (b). Nevertheless, the previously observed outer boundary zones with largest error become smoother, because the target mesh presents elements with an in-plane dimension bigger than the donor mesh, which avoids the extrapolation. Furthermore, the Master-Slave method provides slightly reduced areas of error when compared to Planar, as it benefits from the use of more values along the thickness (z), which are equal for each (r,θ) pair, although both have the extreme values in the same locations. The IVR method presents slightly bigger values of error, specifically in the areas where the target mesh presents smaller in-plane elements and near the zone corresponding to the mesh topology transition.

The histograms of error are shown in Fig. 6 and the corresponding absolute maximum values in Table 2, for both stages and all remapping methods. In *stage 1*, both forms of Dual Kriging interpolation provide identical error distribution for both stages. Moreover, they provide a smaller error dispersion than the IVR method, both in terms of maximum (positive) and minimum (negative) error values. Regarding the error frequency in the *stage 2* (see Fig. 6 (b)), it is possible to conclude that the IVR method exhibits a higher frequency and increased error values. On the other hand, the amplitude of the remapping error is larger for the Planar method than for the Master-Slave.

Concerning *stage 1*, the Master-Slave and the Planar methods present 99% and 98% of the GPs with error value inferior to 0.005, respectively. On the other hand, for the IVR method, about 50% of the GPs present an error smaller than 0.005, and 21% between 0.005 and 0.01. Regarding *stage 2*, the Master-Slave method yields 99% of the GPs with an error smaller than 0.005, while the Planar method provides 98% of all GPs inside this error range. For the IVR method, almost 50% of GPs present error inferior to 0.005. Therefore, the results are similar in terms of error distribution for both stages.

Fig. 7 presents the error distributions obtained with each remapping method for the case with the gradient along the thickness. For *stage 1*, the distribution obtained with the Master-Slave method has the highest spread and error value, while the Planar method presents the lowest.

Furthermore, both the Planar and the IVR methods present only localized areas with increased error, as shown in Fig. 7 (a). In fact, the Planar and the IVR remapping methods present an error distribution similar to the one obtained for the case without through-thickness gradient (see Fig. 5 (a)), but with error values slightly higher.

Regarding *stage 2*, the IVR method presents an error distribution identical to the one obtained in *stage 1*, but with some zones with higher values (see Fig. 7 (b)). The Master Slave's area with increased error values is considerable when compared with the one attained by the other methods. The Planar selection method shows an increase in the error dispersion in comparison with the previous stage. From the error frequency analysis (see Fig. 8), it is possible to conclude that the Master-Slave method presents the highest overall error and spread in both stages, while the Planar selection method had the lowest. The extreme values of the error increase slightly (see Table 3), when comparing with *stage 1,* for both the IVR and the Planar selection methods, while for the Master-Slave the amplitude decreased. Considering the application of the Planar selection method, all GPs had an error inferior to 0.010 in both stages (see Table 3). By applying the IVR method, in *stage 1*, 92% of GPs present an error below 0.010, which reduces to almost 62% when the Master Slave method is adopted. In *stage 2*, these ratios decreased to about 88% and almost 42%, respectively. The absolute maximum values (see Table 3) increased slightly for Planar and IVR, while decreasing for Master-Slave, nevertheless, this method attained the highest error values and worst global results for this case.

By comparing the results obtained for both tests, without and with through-thickness gradient, it can be concluded that the error distribution obtained by the Planar selection method is only slightly affected by the addition of the gradient. The IVR method presents larger zones with increased error values. As for the Master-Slave selection method, the error distribution is strongly affected by the gradient, resulting in a wider spread and higher values. In fact, by adding the thickness gradient, the error distribution frequency and extreme values increased for all methods. However, while the IVR and the Planar selection methods present errors with similar orders of magnitude, the Master-Slave method showed poorer performance in the through-thickness gradient case. This arises from the relative dimensions of the mesh, i.e. the size of the elements is much bigger in the in-plane directions than along the thickness, which leads to an overweighting of the through thickness direction component. It should be mentioned that, when applying the Master-Slave method in the example with the gradient along the thickness direction, the extreme error values occur on the interior GPs. However, as shown in Fig. 7, the GPs located on the surface also present increased error values when compared to the example without the gradient (see Fig. 5 and Fig. 7). Additionally, the maximum absolute errors obtained with Planar and Master-Slave methods in *stage 2* are in the same locations. Comparing both meshes it is clear that the dominating factor for the accuracy is the relative dimension of the elements. The elements in those specific zones in *stage 1* present an higher in-plane dimension than in *stage 2*, leading to a worse capture of the in-plane gradient and, consequently, to an increased error.

3.2. Computational performance

The computational cost associated exclusively with the remapping operation was evaluated and is presented in Table 4, for both examples. For the implemented Dual Kriging methods, it is important to mention that: (i) the Master-Slave method selects a higher number of donor GPs; thus, (ii) the maximum dimension of the Kriging matrix differs, i.e. for the Planar selection

method is 12×12, while for the Master-Slave is 31×31; nonetheless, (iii) the Planar selection method requires the conversion from 3D to a 2D (Planar) coordinate system.

Both Dual Kriging remapping methods are significantly faster than the IVR method, as shown in Table 4. At least 87% of the computational time can be saved for non-matching meshes, i.e. meshes that have no relation between them and, therefore, require an intersection algorithm to identify correspondence between donor and target elements. The existence (or not) of the gradient has no effect on the computational time because the number of operations involved is exactly the same in both cases.

The difference in computational time between *stage 1* and *stage 2* is dictated by the number of GPs that need to be evaluated and the donor mesh density. The former increases the time spent assembling and inverting the Kriging matrices, while the latter increases the time spent searching for the nearest GPs and Master Element. It is also clear that Planar scales comparably to IVR, while Master-Slave differ only slightly with the increase of GPs. Comparing Planar and Master-Slave selection methods, the critical difference is due to the non-linear increase of the time taken assessing the local neighbourhood, and assembling and inverting the Kriging matrix. Albeit a small increase, its effects stack due to the high number of GPs.

The average number of GPs used in each evaluation for the Master-Slave method can be estimated by firstly dividing the target GPs into two groups: internal and surface located GPs (the number of GPs on the edges is negligible). The former have 27 donor GPs available to define the domain, while the latter only have 18 GPs. Thus, the average dimension of the system is 22.5, compared to the average of 9 for the Planar method. This can explain the higher increase of the computational time with the increase of target GPs to be evaluated, obtained for the Master-Slave method when compared with the Planar.

4. Trimming Example

The second example considers a trimming operation, performed on a rectangular specimen that was submitted to a bending operation. This example is selected because it leads to a through-thickness stress gradient similar to the ones that occur in sheet metal forming operations. The springback prediction, which is one of the main sources of geometrical and dimensional inaccuracy in sheet metal formed components, is known to be very sensitive to the accurate evaluation of this gradient (e.g. [44]). Thus, in processes involving trimming operations it is important to minimize the impact of the remapping in its evaluation. The rectangular specimen has a length of 20 mm (40 elements), width of 5 mm (10 elements) and a thickness of 1 mm (2 elements). It is constrained on one side and symmetry conditions are applied on both lateral faces, while a displacement of 10 mm on the free end is applied, as shown in Fig. 9. After this bending operation, the specimen is cut by the plane, also presented in Fig. 9. The geometrical trimming operation was performed with DD3TRIM code using a correction method for the trimmed elements that relocates the nodes associated with the trimmed elements onto the trimming surface [20, 45]. After the trimming process, the remapping of the state variables was performed only on the elements altered by this operation (total of 146 GPs). The results for the von Mises equivalent stress are shown in Fig. 10, comparing the distribution before and after trimming.

Concerning the upper surface of the specimen shown in Fig. 10, only negligible changes are induced by the remapping operation, whatever the method adopted. Furthermore, all methods

display similar distributions along the thickness. Since there is no analytical result for direct comparison of this example, and based on the results for the previous example, the results obtained with the Planar selection method were used as a baseline for comparison. The relative error ER is defined as:

$$ER = \frac{\alpha^{\text{Method}}(\boldsymbol{x}_t) - \alpha^{\text{Planar}}(\boldsymbol{x}_t)}{\alpha^{\text{Planar}}(\boldsymbol{x}_t)}. \quad (11)$$

where α^{Planar} is the value interpolated by the Planar method, in a given target GP with Cartesian coordinates $\boldsymbol{x}_t$, and α^{Method} is the value obtained by either the IVR or the Master-Slave method, in the same GP.

Fig. 11 presents the histogram of the relative error for the trimming example. Both the IVR and the Master-Slave methods provide results that tend to deviate from the ones obtained with the Planar method. As shown in Fig. 10, as expected, the equivalent stress decreases along the length of the specimen (from the fixed support), and from the exterior to the interior (along the thickness direction). Both IVR and Master-Slave methods consider the influence of the GPs that are located near the external surfaces and, consequently, attain slightly higher values for the interior GPs than the Planar method. Therefore, the histogram presents more occurrences on the positive side of the axis (see equation (11)).

The difference between the maximum values given by IVR and Master-Slave is about 1.2%. A total of 113 and 97 GPs are within the 1% range; and 141 and 139 GPs are within the 2% range, respectively for IVR and Master-Slave. At 2.5%, both methods have 144 GPs, the remaining two GPs appear between 2.5% and 3% for the IVR method, and 4% and 4.5% for the Master-Slave. All methods provide good overall results, and thus, can be used in conjunction with a trimming and remapping algorithm.

Table 5 shows the computational time obtained with the remapping methods tested, showing that Dual Kriging interpolation can lead to a quarter of IVR's computational time. The difference between Master-Slave and Planar is small for this case; but, as shown in the previous section, it will increase with the number of GPs that require remapping, i.e. 2% is insignificant for most applications but will be considerable if applied multiple times. Based on other validation tests, the relative proportions will not change significantly up to 5%. These computational time results are representative of the time for adaptive mesh refinement algorithms, where no complex search algorithms are required due to the information regarding the equivalence between old and new finite elements.

5. Conclusions

This work presents the application of the Dual Kriging interpolation method as remapping scheme for FEM state variables between different finite element meshes. Only the standard 8-node hexahedral finite elements are addressed, considering the state variable assigned to the Gauss Points. Since both the computational cost and the accuracy of the Dual Kriging method is influenced by the amount of information used, two different selection algorithms were developed, namely the Master-Slave and Planar. Additionally, the developed remapping method is compared with the IVR method, both in terms of accuracy and computational performance.

For the examples considered in the present study, all remapping methods can provide results with a good level of accuracy. The first example deals with the remapping of an analytical function between finite element meshes with different topology. Assuming there is no gradient of the variable along one direction, the Master-Slave and Planar methods present a significant improvement over the IVR. When considering a state variable distribution with gradient in all directions, combined with a small thickness dimension, a decrease of accuracy is observed for the Master-Slave method, due to an overweighting of the through-thickness component, while the Planar method kept its level of accuracy. Regarding the computational performance, the computational cost incurred for the Dual Kriging is about 15% of the time used in IVR, for non-related meshes; and about 25% for related meshes, such as the ones used in remapping after trimming or remeshing.

6. Acknowledgements

The authors gratefully acknowledge the financial support of the Portuguese Foundation for Science and Technology (FCT) under projects PTDC/EMS-TEC/0702/2014 and PTDC/EMS-TEC/6400/2014. The second author is also grateful to the FCT for the Postdoctoral grant SFRH/BPD/101334/2014.

7. References

1. Thomée V (2001) From finite differences to finite elements. J Comput Appl Math 128:1–54. doi: 10.1016/S0377-0427(00)00507-0

2. Gupta KK, Meek JL (1996) a Brief History of the Beginning of the Finite Element Method. Int J Numer Methods Eng 39:3761–3774. doi: 10.1002/(SICI)1097-0207(19961130)39:22<3761::AID-NME22>3.0.CO;2-5

3. Zienkiewicz OC, Taylor RL, Zhu JZ (2013) The Finite Element Method: its Basis and Fundamentals, 6th ed. Finite Elem Method its Basis Fundam. doi: 10.1016/B978-1-85617-633-0.00020-4

4. Zienkiewicz OC, Taylor RL, Nithiarasu P (2014) The Finite Element Method for Fluid Dynamics. Finite Elem Method Fluid Dyn. doi: 10.1016/B978-1-85617-635-4.00018-2

5. Zienkiewicz OC, Taylor RL, Fox D (2014) The Finite Element Method for Solid and Structural Mechanics. Finite Elem Method Solid Struct Mech. doi: 10.1016/B978-1-85617-634-7.00018-1

6. Chenot J-L, Bernacki M, Bouchard P-O, et al. (2014) Recent and future developments in finite element metal forming simulation. 11th Int. Conf. Technol. Plast. ICTP 2014 81:

7. Veyhl C, Belova IV, Murch GE, et al. (2010) On the mesh dependence of non-linear mechanical finite element analysis. Finite Elem Anal Des 46:371–378. doi: 10.1016/j.finel.2009.12.003

8. Suresh K, Regalla SP (2014) Effect of Mesh Parameters in Finite Element Simulation of Single Point Incremental Sheet Forming Process. Procedia Mater Sci 6:376–382. doi: 10.1016/j.mspro.2014.07.048

9. Shayanfar MA, Kheyroddin A, Mirza MS (1997) Element size effects in nonlinear analysis of reinforced concrete members. Comput Struct 62:339–352. doi: 10.1016/S0045-7949(96)00007-7

10. Schäfer M (2006) Computational engineering: introduction to numerical methods. New York. doi: 10.1007/3-540-30686-2

11. Barros PD, Baptista AJ, Alves JL, et al. (2013) Trimming of 3D solid finite element meshes: sheet metal forming tests and applications. Eng Comput 31:237–257. doi: 10.1007/s00366-013-0344-8

12. Wang D, Randolph MF, White DJ (2013) A dynamic large deformation finite element method based on mesh regeneration. Comput Geotech 54:192–201. doi: 10.1016/j.compgeo.2013.07.005

13. Alves ML, Fernandes JLM, Rodrigues JMC, Martins PAF (2003) Finite element remeshing in metal forming using hexahedral elements. J Mater Process Technol 141:395–403. doi: 10.1016/S0924-0136(03)00388-1

14. Bussetta P, Boman R, Ponthot J-P (2015) Efficient 3D data transfer operators based on numerical integration. Int J Numer Methods Eng 102:892–929. doi: 10.1002/nme.4821

15. Chung SW, Kim SJ (2003) A remeshing algorithm based on bubble packing method and its application to large deformation problems. Finite Elem Anal Des 39:301–324. doi: 10.1016/S0168-874X(02)00075-6

16. Lu B, Ou H (2012) An efficient approach for trimming simulation of 3D forged components. Int J Mech Sci 55:30–41. doi: 10.1016/j.ijmecsci.2011.11.013

17. Jiao X, Heath MT (2004) Common-refinement-based data transfer between non-matching meshes in multiphysics simulations. Int J Numer Methods Eng 61:2402–2427. doi: 10.1002/nme.1147

18. Hinton E, Campbell JS (1974) Local and global smoothing of discontinuous finite element functions using a least squares method. Int J Numer Methods Eng 8:461–480. doi: 10.1002/nme.1620080303

19. Perić D, Hochard C, Dutko M, Owen DRJ (1996) Transfer operators for evolving meshes in small strain elasto-placticity. Comput Methods Appl Mech Eng 137:331–344. doi: 10.1016/S0045-7825(96)01070-5

20. Baptista AJC (2006) Mechanical Modelling and Numerical Simulation of the Multi-Step Sheet Metal Forming Process. Dissertation, University of Coimbra

21. Rashid MM (2002) Material state remapping in computational solid mechanics. Int J Numer Methods Eng 55:431–450. doi: 10.1002/nme.508

22. Zienkiewicz OC, Zhu JZ (1992) The superconvergent patch recovery (SPR) and adaptive finite element refinement. Comput Methods Appl Mech Eng 101:207–224. doi: 10.1016/0045-7825(92)90023-D

23. Kwak D-Y, Im Y-T (2002) Remeshing for metal forming simulations—Part II: Three-dimensional hexahedral mesh generation. Int J Numer Methods Eng 53:2501–2528. doi: 10.1002/nme.404

24. Margolin LG, Shashkov M (2003) Second-order sign-preserving conservative interpolation (remapping) on general grids. J Comput Phys 184:266–298. doi: 10.1016/S0021-9991(02)00033-5

25. Farhat C, Lesoinne M, Le Tallec P (1998) Load and motion transfer algorithms for fluid/structure interaction problems with non-matching discrete interfaces: Momentum and energy conservation, optimal discretization and application to aeroelasticity. Comput Methods Appl Mech Eng 157:95–114. doi: 10.1016/S0045-7825(97)00216-8

26. Luce R, Wolske M, Kopp R, et al. (2001) Application of a dislocation model for FE-process simulation. Comput Mater Sci 21:1–8. doi: 10.1016/S0927-0256(00)00210-X

27. Ortiz M, Quigley JJ (1991) Adaptive mesh refinement in strain localization problems. Comput Methods Appl Mech Eng 90:781–804. doi: 10.1016/0045-7825(91)90184-8

28. Dukowicz JK, Baumgardner JR (2000) Incremental Remapping as a Transport/Advection Algorithm. J Comput Phys 160:318–335. doi: 10.1006/jcph.2000.6465

29. Bochev P, Shashkov M (2005) Constrained interpolation (remap) of divergence-free fields. Comput Methods Appl Mech Eng 194:511–530. doi: 10.1016/j.cma.2004.05.018

30. Baptista AJ, Alves JL, Oliveira MC, et al. (2007) Incremental volumetric remapping method: Analysis and error evaluation. NUMIFORM ’07 Mater Process Des Model Simul Appl Pts I II 908:835–840.

31. Baptista AJ, Alves JL, Oliveira MC, et al. (2005) Application of the Incremental Volumetric Remapping Method in the Simulation of Multi-Step Deep Drawing Processes. In: AIP Conf. Proc. AIP, pp 173–178

32. McLean P, Léger P, Tinawi R (2006) Post-processing of finite element stress fields using dual kriging based methods for structural analysis of concrete dams. Finite Elem Anal Des 42:532–546. doi: 10.1016/j.finel.2005.10.004

33. Ulaganathan S, Couckuyt I, Dhaene T, et al. (2015) Performance study of gradient-enhanced Kriging. Eng Comput. doi: 10.1007/s00366-015-0397-y

34. Toal DJJ (2015) A study into the potential of GPUs for the efficient construction and evaluation of Kriging models. Eng Comput. doi: 10.1007/s00366-015-0421-2

35. Wong FT, Kanok-Nukulchai W (2009) Kriging-Based Finite Element Method : Element-By-Element Kriging Interpolation. Civ Eng Dimens 11:15–22.

36. Grandy J (1999) Conservative Remapping and Region Overlays by Intersecting Arbitrary Polyhedra. J Comput Phys 148:433–466. doi: 10.1006/jcph.1998.6125

37. Hughes TJR (1980) Generalization of selective integration procedures to anisotropic and nonlinear media. Int J Numer Methods Eng 15:1413–1418. doi: 10.1002/nme.1620150914

38. Krige DG (1976) A review of the development of geostatistics in South Africa. In: Adv. geostatistics Min. Ind. Springer Netherlands, Dordrecht, pp 279–293

39. Matheron G (1976) Les Concepts de Base et L'Evolution de la Geostatistique Miniere. In: Adv. Geostatistics Min. Ind. Springer Netherlands, Dordrecht, pp 3–10

40. Poirier C, Tinawi R (1991) Finite element stress tensor fields interpolation and manipulation using 3D dual kriging. Comput Struct 40:211–222. doi: 10.1016/0045-7949(91)90348-P

41. Trochu F (1993) A contouring program based on dual kriging interpolation. Eng Comput 9:160–177. doi: 10.1007/BF01206346

42. Diogo CMA (2015) DD3TRIM - Revised and Augmented Version. Dissertation, University of Coimbra

43. Coll A, Ribó R, Pasenau M, et al. (2014) GiD v.12 User Manual.

44. Wagoner R, Li M (2007) Simulation of springback: Through-thickness integration. Int J Plast 23:345–360. doi: 10.1016/j.ijplas.2006.04.005

45. Baptista AJ, Alves JL, Rodrigues DM, Menezes LF (2006) Trimming of 3D solid finite element meshes using parametric surfaces: Application to sheet metal forming. Finite Elem Anal Des 42:1053–1060. doi: 10.1016/j.finel.2006.03.005

Figure 1

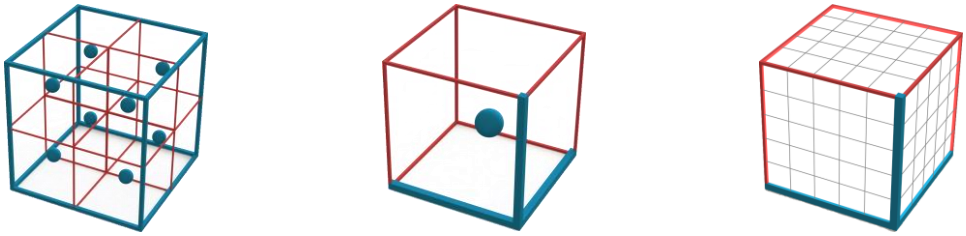

(a) (b) (c)

Fig. 1 Subdivision of the finite element mesh. (a) Element partition in Gauss Volumes (GPs in blue circles); (b) single Gauss Volume; (c) Partition of the target Gauss Volume in nl^3 equal subdivisions in each direction (Adapted from [30])

Figure 2

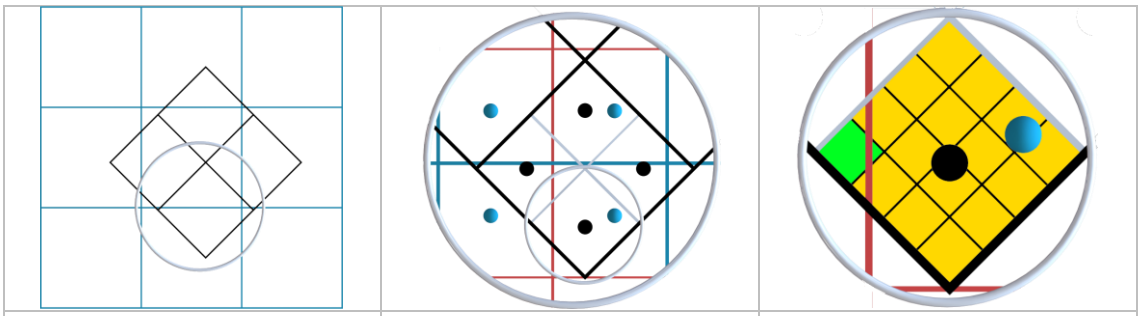

Fig. 2 2D schematic of the IVR method with donor (blue) and target (black) meshes: (a) detail of one target element; (b) partition of the donor and target elements into Gauss Volumes and detail of one target Gauss Volume; (c) partition of the target Gauss Volume in nl^3 subvolumes and evaluation of each donor Gauss Volume (Adapted from [30])

Figure 3

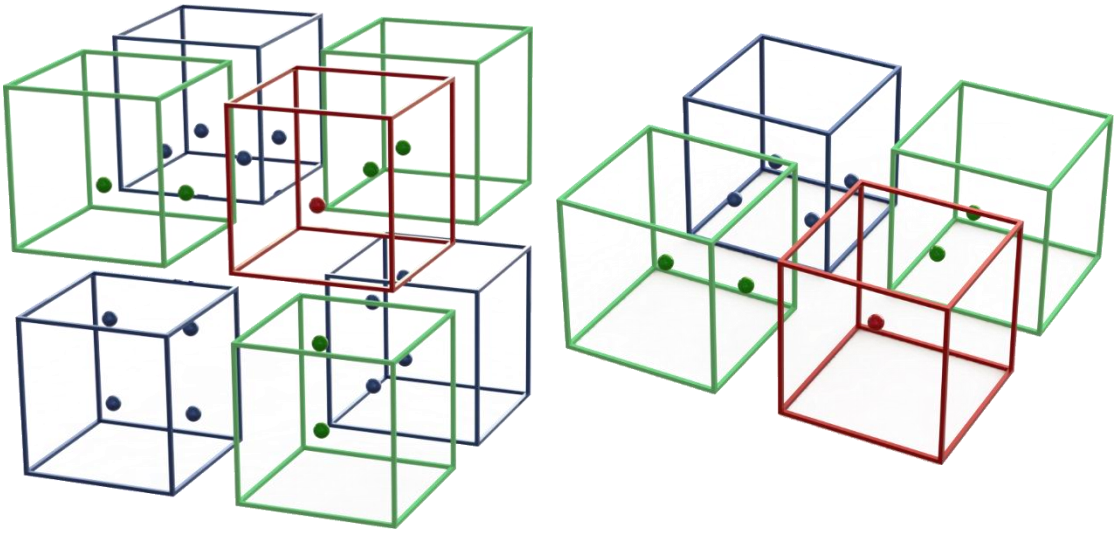

(a) *(b)*

Fig. 3 Comparison of donor GPs' sets for both Kriging methods, for a target node located in the left bottom quadrant: (a) Master-Slave method (Master Element and its eight GPs are omitted); (b) Planar selection method

Figure 4

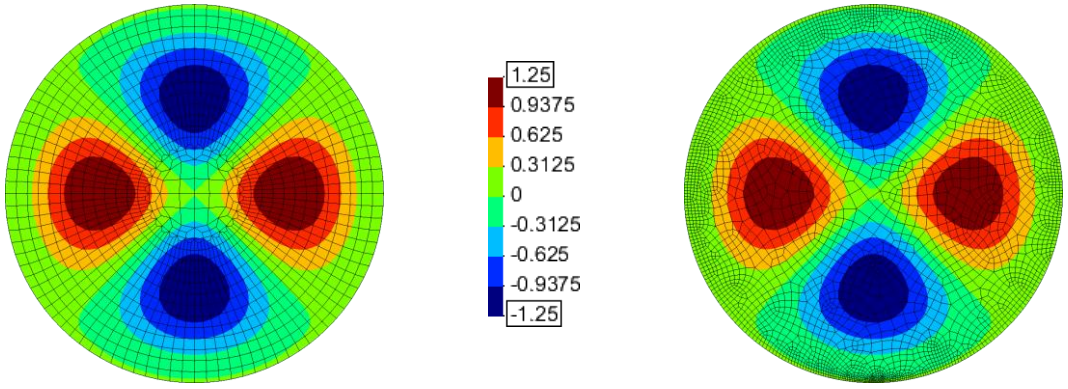

(a) (b)

Fig. 4 Scalar variable distribution on both finite element meshes (2 layers through the thickness): (a) Mesh 1 composed by 2 688 elements (21 504 GPs) and 4 179 nodes; (b) Mesh 2 composed by 6 694 elements (53 552 GPs) and 10 575 nodes

Figure 5

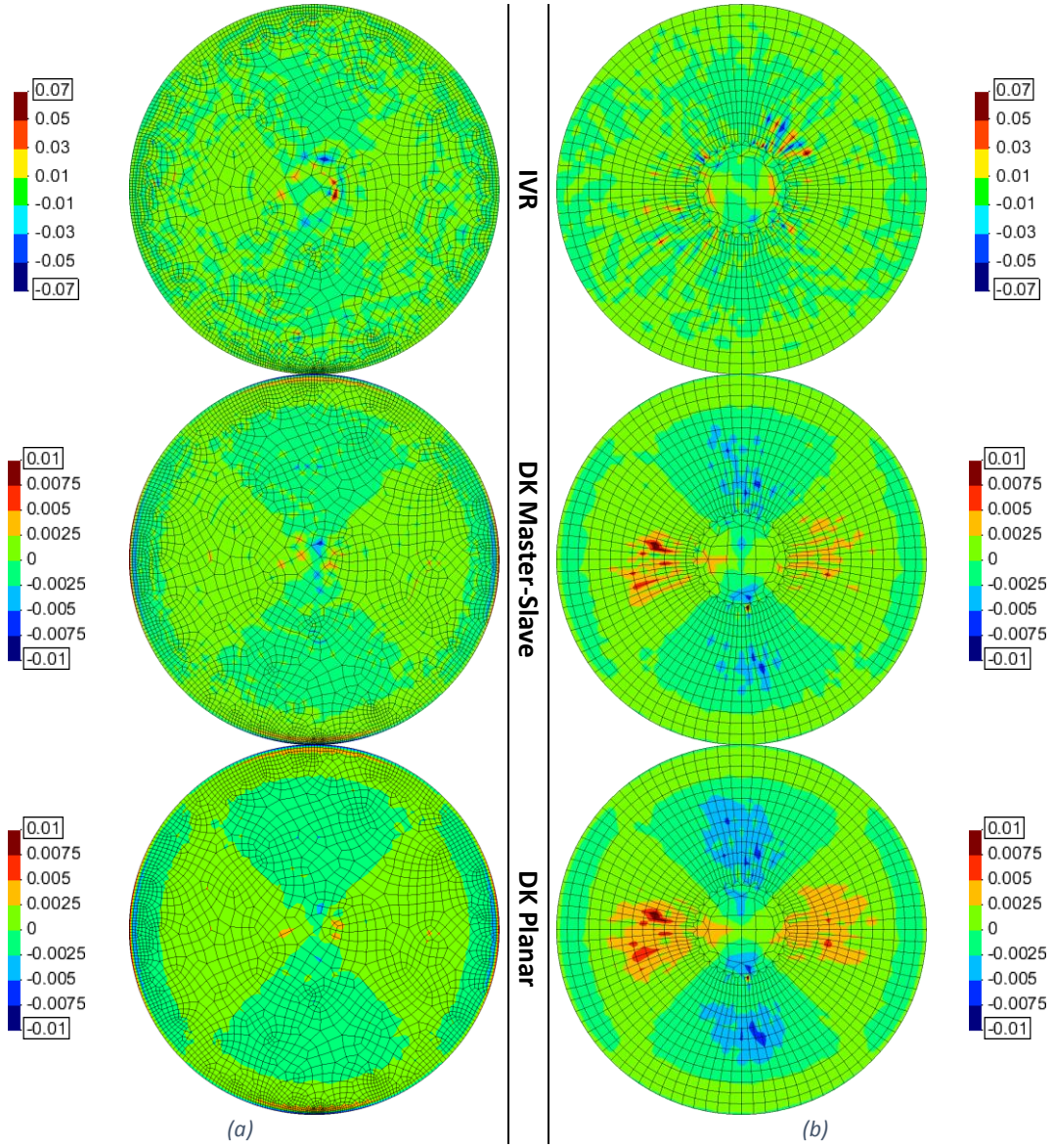

Fig. 5 Distributions of error: Incremental Volumetric Remapping (IVR), Dual Kriging Master-Slave and Planar Dual Kriging. Case without through-thickness gradient: (a) Stage 1 and (b) Stage 2

Figure 6

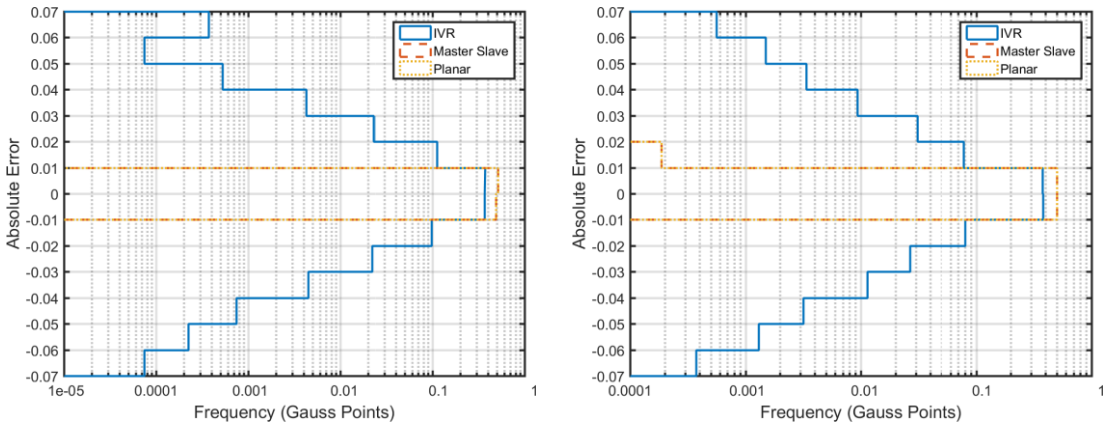

Fig. 6 Histograms of the error in the remapping for the case without through-thickness gradient: (a) Stage 1; (b) Stage 2

Figure 7

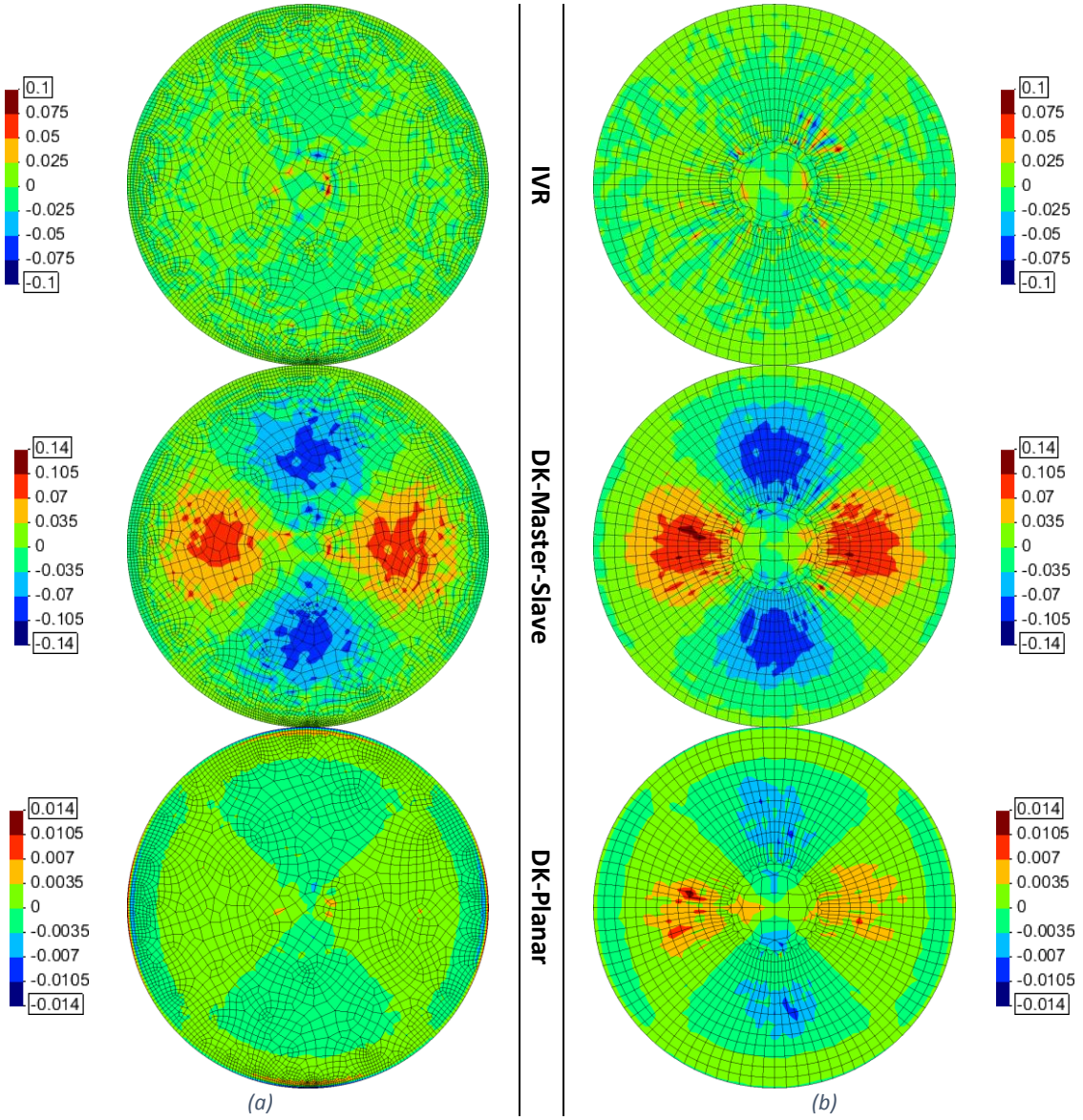

Fig. *7* Distributions of error: Incremental Volumetric Remapping (IVR), Dual Kriging Master-Slave and Planar Dual Kriging. Case with through-thickness gradient: (a) Stage 1 and (b) Stage 2

Figure 8

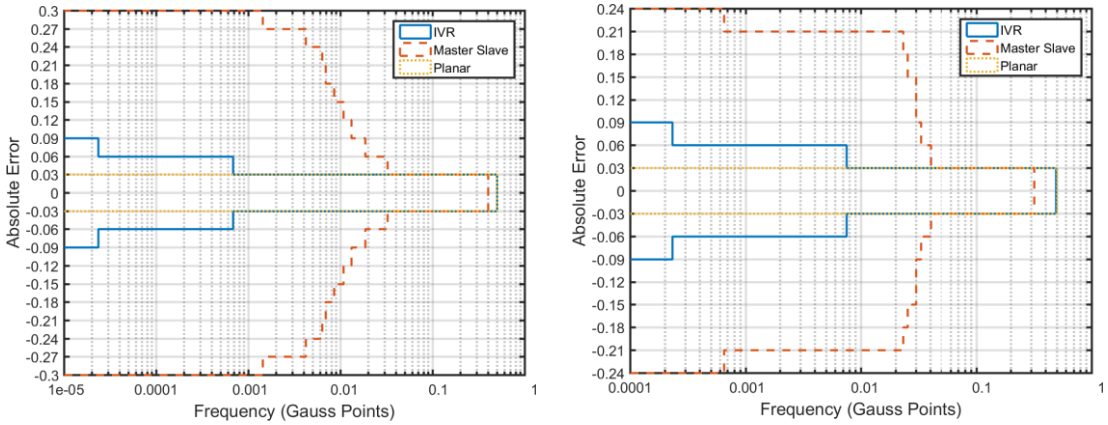

Fig. 8 Histograms of the error in the remapping for the case with through-thickness gradient: (a) Stage 1; (b) Stage 2

Figure 9

Fig. 9 Schematic representation of the specimen configuration after the bending operation, including the trimming plane

Figure 10

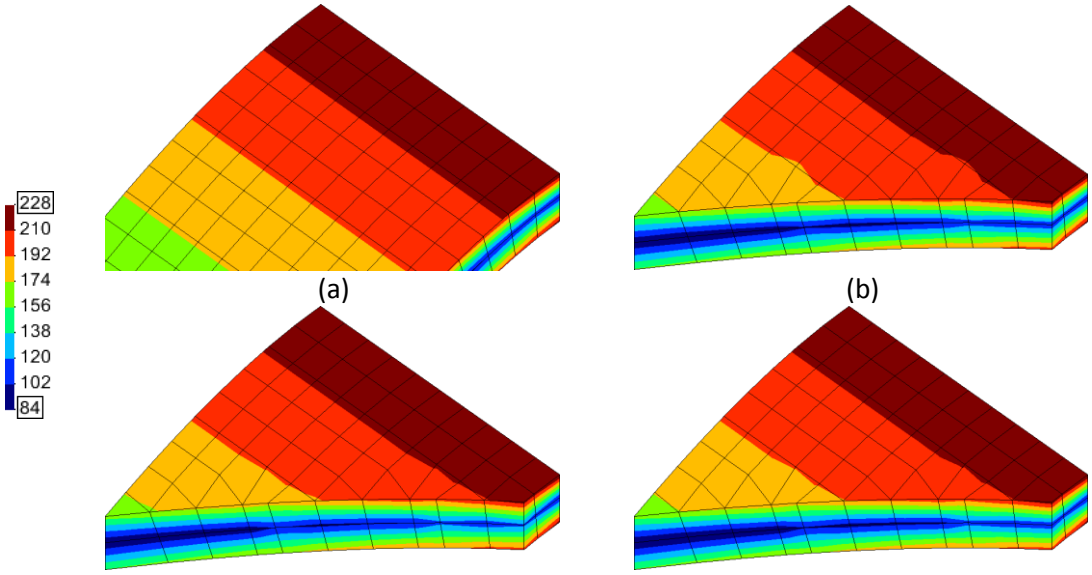

Fig. 10 Distribution of the equivalent stress after the bending operation ((a) Original) and after the trimming operation, as obtained with the Incremental Volumetric Remapping ((b) IVR), Dual Kriging Master-Slave (c) and Planar Dual Kriging (d)

Figure 11

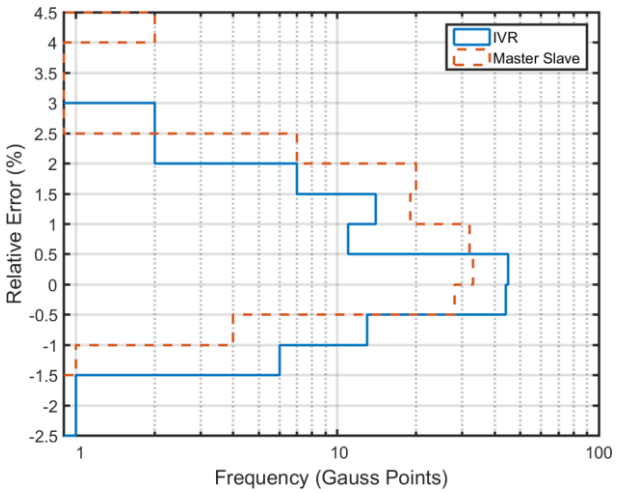

Fig. 11 Histograms of the relative error in the remapping of the equivalent stress obtained in the bending test, after the trimming operation (total of 146 target GPs)

Table 1*:* Nomenclature adopted in the selection methods used in the Kriging method

Name	Definition
Master Node	Closest node from the donor mesh to the target GP
Master Element	Donor mesh's element partially defined by the Master Node, containing the target GP
Master GPs	Donor mesh's GPs belonging to the Master Element
Slave Elements	Donor mesh's elements that share the Master Node, but do not contain the target GP
Slave GPs	Donor mesh's GPs that belong to any Slave Element, which will be considered in the Dual Kriging process.

Table 2

Table 2: Maximum error values for the case without through-thickness gradient

Stage 1		Error	Stage 2		Error
IVR	Max	0.0666	**IVR**	Max	0.0624
	Min	-0.0720		Min	-0.0720
Master-Slave	Max	0.0072	**Master-Slave**	Max	0.0103
	Min	-0.0093		Min	-0.0074
Planar	Max	0.0072	**Planar**	Max	0.0108
	Min	-0.0093		Min	-0.0078

Table 3

Table 3: Maximum values for the case with through-thickness gradient

Stage 1		Error	Stage 2		Error
IVR	Max	0.0621	**IVR**	Max	0.0682
	Min	-0.0621		Min	-0.0682
Master-Slave	Max	0.2940	**Master-Slave**	Max	0.2256
	Min	-0.2940		Min	-0.2256
Planar	Max	0.0093	**Planar**	Max	0.0097
	Min	-0.0093		Min	-0.0097

Table 4: Computational time and relative difference of the Dual Kriging methods to IVR

	Time (s)	**Time (s)**	**Time (s)**
Operation	**IVR ($nl = 5$)**	**Master-Slave**	**Planar**
With Gradient			
Stage 1	216	29 (13%)	23 (11%)
Stage 2	197	24 (12%)	22 (11%)
Without Gradient			
Stage 1	216	29 (13%)	23 (11%)
Stage 2	197	24 (12%)	22 (11%)

Average time for 12 executions on an i7-4860HQ 2.40-3.20 GHz, always discarding two extreme values. Values rounded.

Table 5

Table 5: Computational Time and relative difference of the Dual Kriging methods to IVR: Trimming Example

Operation	**IVR (nl=5)**	**Master-Slave**	**Planar**
Remapping Step	4.47	1.13 (25.2%)	1.06 (23.7%)

Average time for 12 executions on an i7-4860HQ 2.40-3.20 GHz, always discarding two extreme values.